Materials and Design 112 (2016) 131–139

Contents lists available at ScienceDirect

Materials and Design

journal homepage: www.elsevier.com/locate/matdes

Combinatorial screening of the microstructure–property relationships for Fe–B–X stiff, light, strong and ductile steels

C. Baron, H. Springer *, D. Raabe

Max-Planck-Institut für Eisenforschung GmbH, 40237 Düsseldorf, Germany

HIGHLIGHTS

- Systematic screening of mechanical, physical and microstructural properties of Fe–10B–5X alloys for lightweight design
- Ti, Zr, Hf, V, Nb, Ta, Cr, Mo, W additions exhibit widely differing microstructures of different boride phases and mixes
- Cr and Zr were identified as the most promising elements for design of high modulus steels
- Fe–B–Cr alloys exhibit similar performance as the established Ti alloyed materials, but at greatly reduced alloying costs
- Zr alloyed materials are softer and less ductile, but achieve extremely high stiffness/density ratio

GRAPHICAL ABSTRACT

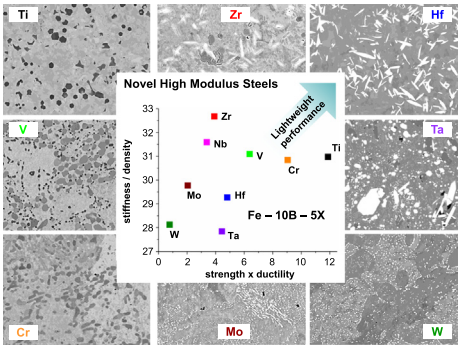

ARTICLE INFO

Article history:
Received 25 August 2016
Received in revised form 13 September 2016
Accepted 18 September 2016
Available online 20 September 2016

Keywords:
Steel
Lightweight design
Strength
Density
Stiffness
Ductility

ABSTRACT

We systematically screened the mechanical, physical and microstructural properties of the alloy systems Fe–10 B–5 X (at.%; X = Ti, Zr, Hf, V, Nb, Ta, Cr, Mo, W), in order to identify novel metal matrix composite steels as next generation lightweight materials. The alloys were synthesised and processed by bulk liquid metallurgical techniques, and subsequently analysed for their mechanical and physical properties (i.e. Young's modulus, density, tensile strength and ductility) as well their microstructure and constitution. From the wide variety of observed boride phases and microstructures and resultant different properties, Cr and Zr additions were found to be most effective. Cr qualifies well as the high fraction of M_2B borides of spherical morphology allows achieving a similar stiffness/density ratio and mechanical performance as the reference Ti alloyed materials, but at substantially reduced alloy costs. Zr blended composites on the other hand are softer and less ductile, but the alignment of spiky ZrB_2 particles during swaging led to a much higher – though most probably anisotropic – specific modulus. Consequences and recommendations for future alloy and processing design are outlined and discussed.

1. Introduction

Weight reduction is a major technical challenge for structural material design. An ideal pathway is blending strong and ductile metallic matrices for optimised mechanical performance with stiff and low-density ceramic particles for improved physical properties, thus creating metal

* Corresponding author.
E-mail address: h.springer@mpie.de (H. Springer).

http://dx.doi.org/10.1016/j.matdes.2016.09.065
0264-1275/

matrix composites [1–6]. Key material parameters are a high Young's modulus (E) for improved stiffness, high yield strength (YS) to allow for higher loads to be transferred, satisfactory ductility (such as tensile elongation TE) for forming operations during manufacturing, and a low density (ρ). High modulus steels (HMS; as the most common acronym for iron (Fe)-based composites) are especially attractive, as Fe exhibits a similar specific modulus (E/ρ) as established lightweight materials such as for example aluminium, magnesium or titanium alloys (about 26 GPa g^{-1} cm^3), but also a wide range of achievable mechanical properties due to its multitude of equilibrium and non-equilibrium phase transformations and low production costs [7].

Selecting suited particle phases however – from intrinsic properties alone – is difficult, as possible candidates are numerous and range from carbides to nitrides, oxides, intermetallics and borides [1]. Besides high efficiency (i.e. a high specific modulus), other aspects of critical importance are e.g. their thermodynamic stability (to prevent dissolution in the matrix), formation kinetics (possible floatation of low density particles forming in the liquid), interfacial properties (to ensure wetting of particles), as well as the availability and costs of the constituting elements. Furthermore, in-situ formation of such particles during synthesis greatly simplifies the production of such composite materials. All these factors are important for liquid metallurgy synthesis, and thus of key relevance for efficient mass production. When reviewing the wide range of stiff and low density particles under these engineering constraints, only a limited number of possible phases remain: Diamond for example has one of the highest specific moduli, but cannot be synthesised in-situ and will dissolve in Fe when added ex-situ. By contrast nitrides or oxides have high thermodynamic stability, but as they form rapidly in the melt and are typically of low mass density, they float and form a slag instead of rendering dispersed in the solidified material [8]. Carbides are typically less effective, and detrimental for both the mechanical properties (through preferential precipitation at grain boundaries) and the melt viscosity (formation in the liquid phase) [4].

Borides, on the other hand, fulfill most of the above listed criteria for HMS design. Specifically the Fe–Titanium diboride (TiB_2) system has been intensely investigated [4,8–25], as TiB_2 has a high specific modulus (~125 GPa g^{-1} cm^3) [26] and can be precipitated in-situ from a homogeneous Fe–Ti–B melt in a pseudo-binary eutectic reaction [9], with excellent interfacial properties and sufficient mechanical compliance with the matrix [11,18,23]. An Fe–10 vol.% TiB_2 alloy for example typically exhibits a specific modulus of about 30 GPa g^{-1} cm^3 at 400 MPa and ~30% TE [27,28]. The increased costs associated with the comparatively large quantities of Ti required (about 5 wt.% for the above mentioned alloy) can be decreased by the in-situ reduction of Ti-oxides through aluminium additions in the melt [8]. More problematic is the pronounced embrittlement observed with increasing TiB_2 fractions. This is caused by the unfavourable particle microstructure once the eutectic TiB_2 concentration (about 12 vol.% [20,25]) is exceeded and formation of large (several μm^2) primary particles in addition to the already sharp edged eutectic TiB_2 lamellae occurs. While the particle morphology can be successfully controlled by alloying additions and/or tailored solidification kinetics, leading to excellent property profiles [22,24,27], these measures further increase the associated efforts and costs, and thus may slow down the application of HMS as the next generation lightweight material on a broad scale.

However, as HMS still represent a relatively novel class of structural materials, the potential of other Fe–boride systems has not yet been investigated and exploited. Compared to the more thoroughly studied Fe–TiB_2 based HMS, these alternative alloy systems may offer more effective boride particles (so that lower particle fractions are required for the same gain in properties), and/or improved boride microstructures even with established alloying and processing routes (allowing for improved mechanical performance at similar particle fractions). Identifying the most suitable Fe–B–X system for the design of HMS from existing literature alone is difficult though, for the following reasons: (i) The thermodynamics of the Fe-rich corners of ternary Fe–B–X systems are often not fully understood, thus making it difficult to reliably predict which phases are stable for a specific alloy composition and temperature [29]. (ii) Depending on the alloy system, a multitude of equilibrium phases occurs, with often closely spaced compositional ranges. In the Fe–B–Cr system for example, 9 binary and 6 ternary borides have been reported, not even counting metastable phases which are out of thermodynamic equilibrium [30]. (iii) Apart from the difficulties in predicting the formation of specific phases, data concerning their intrinsic properties (such as E and ρ) is rather scarce. Additionally, almost no information exists on what kind of particle microstructures (i.e. morphology, size and dispersion of the borides) will result for different processing conditions. Hence the prediction of the physical and mechanical performance of such an HMS alloy, i.e. its specific modulus, strength and ductility, is virtually impossible.

An experimental approach, i.e. screening the constitution, microstructure, mechanical and physical properties of ternary Fe–B–X systems, on the other hand, is extremely time consuming in view of the large number of possible alloy compositions and thermomechanical processing parameters, even with novel high throughput bulk metallurgical techniques [31]. Thin film combinatorial techniques may be substantially faster, but the correlation lengths of the property-dominating microstructural features (grain size, crystallographic texture, precipitate dispersion and topology etc.) typically exceed the dimensions accessible in thin films. It is therefore of high interest to use an alternative experimental strategy to efficiently obtain insight into which ternary Fe–B–X system has the highest potential for future HMS alloy design.

2. Objective and approach

The aim of this study is to evaluate ternary Fe–B–X alloy systems for the design of stiff, light, strong and ductile HMS. In view of the above listed difficulties with identifying the most suitable system exclusively from literature data, we follow here a property driven approach, i.e. first producing material based on the available data, then evaluate its mechanical and physical properties, followed by investigation of microstructure and constitution. This allows us to efficiently provide first insights into the underlying microstructural reasons for different types of material behaviour, and to successfully identify the most promising alloy systems for conducting more detailed follow-up studies.

The boride forming elements Ti (as a reference case), zirconium (Zr), hafnium (Hf), vanadium (V), niobium (Nb), tantalum (Ta), chromium (Cr), molybdenum (Mo) and tungsten (W) were selected as compositional variables for this study. It is well known that diborides of the type MB_2 have a great potential as effective high-stiffness phases, as they assume a hexagonal lattice of the type $P6/mmc$, whose close crystallographic packing typically ensures high E values [26,32]. For the systems Fe–B–Ti, Fe–B–Zr and Fe–B–Hf the formation of such MB_2 has been experimentally reported [9], while for example in the case of the Fe–B–Cr system borides of the type M_2B are more likely to form [30]. However, as noted above, as no clear and comparable information exists for the exact thermodynamics of any of the Fe–B–X systems studied here, we chose in this first evaluation step to keep the X/B ratio fixed at 1:2, in order to allow – at least from a stoichiometric standpoint – for the formation of MB_2 type borides. In binary Fe–B alloys Fe_2B is well known to form. While its spherical morphology has shown to be not detrimental for the ductility of the bulk composite [8], its comparatively low stiffness and high density (ρ 7.15 g cm^{-3}, E 290 GPa, respectively [4]) makes it not a promising particle phase for HMS design.

All alloys were synthesised and processed by standard liquid metallurgical techniques, and subsequently analysed regarding their mechanical and physical properties (i.e. E, ρ, YS, TE) as well their microstructure and constitution. The results aim at representing the basis to identify the most suitable systems for alloy design of novel HMS, whose alloy composition and thermomechanical parameters can be most effectively

Table 1
Target and actual chemical compositions (at.%) determined by wet chemical analyses of all alloys of this study in at.% (Fe as balance). Compositional scatter indicates inhomogeneities probably caused by density-induced separation (floating or sinking) of formed boride phases prior to solidification.

Target values/at.%	Actual values/at.%
Fe–10B–5Ti	Fe–11.5B–5.1Ti
Fe–10B–5Zr	Fe–10.9B–4.7Zr
Fe–10B–5Hf	Fe–(10.2–10.3)B–(5.1–5.4)Hf
Fe–10B–5V	Fe–(9.3–10.6)B–(4.3–4.8)V
Fe–10B–5Nb	Fe–10.4B–(5.0–5.2)Nb
Fe–10B–5Ta	Fe–9.6B–4.9Ta
Fe–10B–5Cr	Fe–10.5B–5.2Cr
Fe–10B–5Mo	Fe–9.7B–4.2Mo
Fe–10B–5W	Fe–9.7B–(2.6–2.7)W

studied and refined further by using established high throughput bulk metallurgical techniques [31,33–35].

3. Materials and methods

All alloys of this study are of the composition Fe–10 B–5 X (at.%; X = Ti, Zr, Hf, V, Nb, Ta, Cr, Mo, W). This represents a hypo-eutectic concentration for the reference alloy with Ti, which is an optimum benchmark for judging the performance of the other material systems, as it does not undergo strong embrittlement through the formation of coarse primary particles, and represents the current state of the art in HMS design. Charges of ~600 g were synthesised by Arc melting pure materials (>99.99%) in an Argon atmosphere on a water-cooled copper (Cu) hearth and subsequently cast in a cylindrical Cu mould with 20 mm internal diameter. The chemical compositions (target and actual values determined by wet chemical analysis) are listed in Table 1. Compositional scatter indicates inhomogeneities probably caused by density-induced separation (floating or sinking) of boride phases formed prior to complete solidification. The cast rods were then lathed to 18 mm diameter and hot swaged at 1100 °C to 10 mm diameter followed by air cooling to room temperature. Lathing was utilised to produce cylindrical samples of 9 mm diameter and 45 mm in length for subsequent analysis.

Mass density ρ was measured both on the bulk cylindrical samples (dividing mass by volume; ρ_{bulk}) as well as on flakes collected from lathing with a gas pycnometer (Archimedes technique; ρ_{flakes}) under Ar atmosphere (Micromeritics Accupyc 1330). Sonic induced *E* measurements were conducted with a GrindoSonic Mk5 "Industrial" (indirect measurements following the excitation and resonance method, using flexural vibrations). Tensile testing was performed on small dog-bone shaped samples (gauge length 5 mm, cut by spark erosion parallel to the swaging direction) at an initial strain rate of 10^{-3} s^{-1} and digital image correlation (software Aramis V6.3.0) to map the strain.

Microstructural characterisation was carried out on cross sections prepared in the plane perpendicular to the swaging direction by grinding and polishing using standard metallographic techniques. Imaging was performed with scanning electron microscopy (SEM; Zeiss 1540XB). Phase identification was performed via X-ray diffraction (XRD; Seifert Type ID3003, cobalt radiation, Meteor0D – energy dispersive point detector, 2 mm beam diameter). The Pawley method was used to fit peaks of specific phases (database Bruker Topas V5.0 software) to those of the measured spectra.

4. Results

4.1. Physical and mechanical properties

The *E* and ρ data obtained for the Fe–10 B–5 X alloys are plotted in Fig. 1. In the as-cast state (Fig. 1a), the Mo alloyed samples exhibited with 221 GPa the lowest *E* values (black rhombi), and the Nb alloyed material with 246 GPa the highest ones. The bulk mass density ρ_{bulk} (blue circles) was found to be lowest for the Ti alloyed materials (7.38 g cm^{-3}) and highest for Ta-alloyed samples (8.28 g cm^{-3}). The ρ_{flakes} values (empty red circles) were almost identical to the ρ_{bulk} data except for Nb, Ta and W alloyed materials, where the ρ_{flakes} was about 0.15 g cm^{-3} larger than the respective ρ_{bulk} values. After swaging (Fig. 1b) both ρ and *E* changed substantially. With 227 GPa the lowest *E* was measured for the W alloyed samples, and with 246 GPa the highest for the Zr alloyed material. Similar to the as-cast state, ρ_{bulk} was measured lowest for the Ti alloyed samples (7.40 g cm^{-3}) and highest for Ta alloyed samples (8.33 g cm^{-3}). The differences between ρ_{flakes} and ρ_{bulk} values are now slightly larger. As ρ_{bulk} represents the more realistic mass density values (i.e. those relevant for a manufactured, load bearing machine component) because it includes also possible internal defects such as pores and cracks, we base all the following evaluations on the ρ_{bulk} values, as well as on the *E* values obtained after swaging of the materials for the same reason. In Fig. 2 the determined *E* values of all alloys after swaging are plotted as function of the inverse ρ_{bulk} data (i.e. specific volume). It becomes clear that the Cr, V, Ti, Nb and especially Zr alloyed materials have higher specific modulus (positioned in the upper right corner) than those alloyed with Hf, Mo, Ta and W (bottom left).

The corresponding mechanical performance of all materials in the as-swaged state is shown in Fig. 3 as representative engineering stress/strain curves obtained by tensile testing. Ultimate tensile strength (UTS), YS and especially TE values vary greatly between the

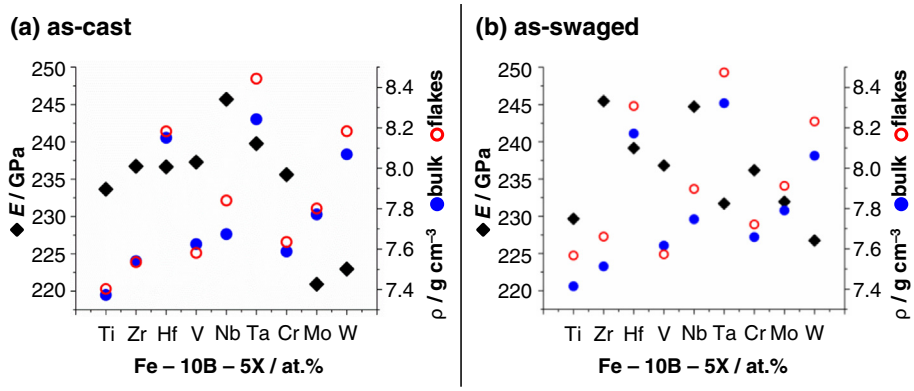

Fig. 1. Young's modulus (*E*) and mass density (ρ) measured on bulk cylindrical samples (dividing mass by volume, ρ_{bulk}) and lathed flakes (Archimedes technique; ρ_{flakes}) for the different alloys in as-cast (a) and as-swaged condition (b).

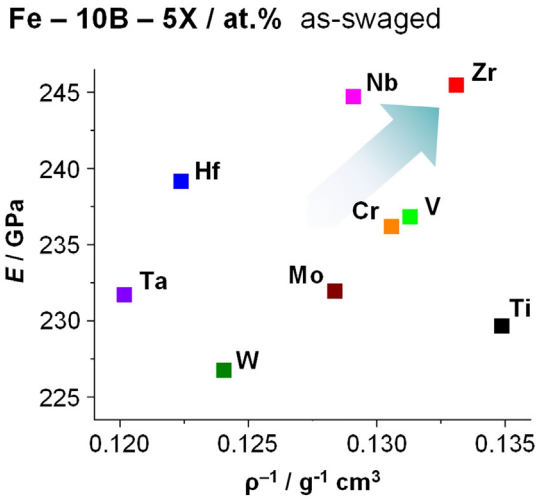

Fig. 2. Young's modulus (E) as function of the inverse ρ_{bulk} data (i.e. specific volume) of the different alloys in as-swaged condition. Materials with a high specific modulus (stiffness/density ratio) are found in the upper right, with a low the specific modulus in the lower left corner, respectively.

different Fe–10 B–5 X alloys. The highest YS was obtained for Mo and W alloyed samples (about 650 MPa), but they fail brittle without noticeable plastic deformation and the TE values are below 3%. The reference Ti alloyed material exhibits with about 30% the largest TE values at intermediate YS (about 420 MPa) and UTS (about 580 MPa). All other alloys show TE values between about 5 and 20% at YS values in the range of 300 and 450 MPa. Interestingly, the Zr alloyed material with the highest specific modulus is the plastically softest one of all tested materials (YS 300 MPa), yet, it is not the most ductile (TE 13%) alloy. This surprising observation underlines the relevance of testing both physical and mechanical performance to evaluate a given alloy system. The mechanical performance of all alloys is summarised in Fig. 4, where the YS of all materials is plotted as a function of their respective TE values (all data points represent average of three test each). A typical inverse strength/ductility relationship can be observed, with the Cr and Ti alloyed material representing positive (i.e. more strong and ductile), the Zr alloyed material negative exceptions (i.e. more soft and brittle).

4.2. Microstructure and constitution

Fig. 5 shows SEM micrographs of the microstructures of all alloys in as-swaged condition in backscatter electron contrast at identical

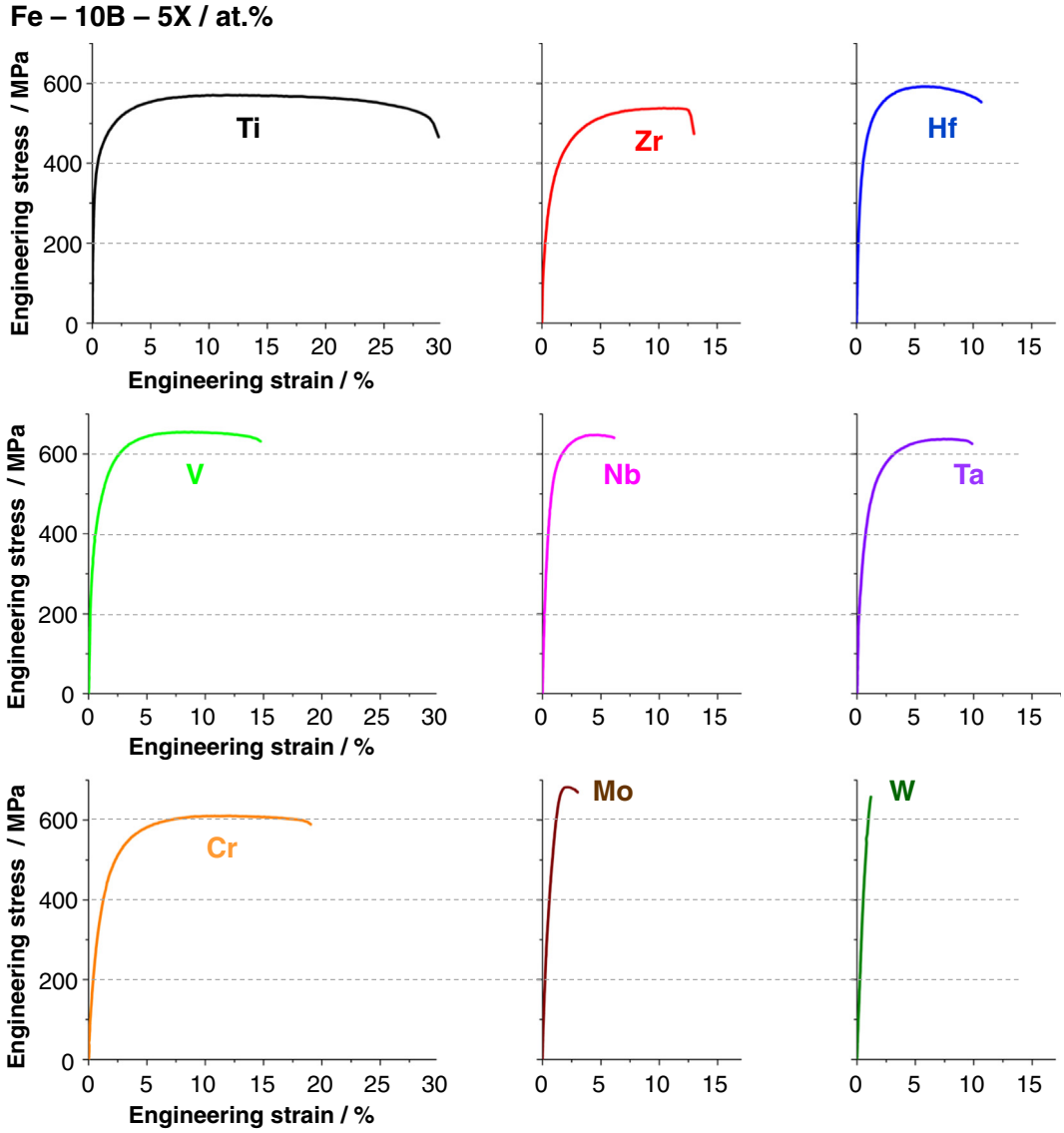

Fig. 3. Engineering stress-strain plots from tensile testing of the different alloys in as-swaged condition.

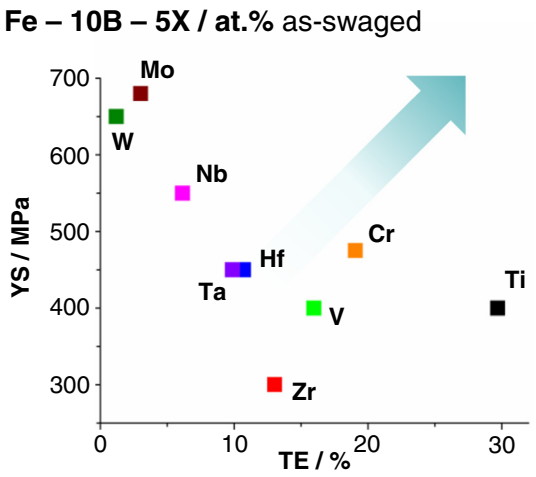

Fig. 4. Yield strength (YS) as a function of total elongation (TE) of the different alloys in as-swaged condition. Materials with high mechanical performance are found in the upper right, with a low the strength and ductility in the lower left corner, respectively.

magnification. While in all Fe–10 B–5 X materials a roughly comparable fraction of particles is found, their contrast, size distribution and morphology varies substantially between the different alloys. The particles are homogeneously distributed for Ti, Hf, Ta and Cr alloyed samples, whereas in Zr and V alloyed samples clustering occurs, and Nb, Mo and W alloyed samples show partly interconnected networks. In the reference Ti alloyed samples hexagonal and irregular shaped black particles of about 2–3 μm diameter can be observed, as it is well known from hypo-eutectic Fe–TiB_2 HMS. Zr-alloyed samples exhibit sharp-edged and elongated light grey particles with about 5–10 μm in length and <2 μm wide, as well as lower amounts of irregular but rounded dark grey particles. In Hf-alloyed samples similar spiky reinforcements in bright contrast with a length from 3 to 10 μm and a width of around 1 μm appear. V and Cr alloyed materials exhibit dark grey, spherical particles with a diameter below 4 μm, yet, the V alloyed samples contain additionally a lower number of smaller and black ellipsoidal particles below 1 μm in width. In Nb alloyed samples bright particles of both larger hexagonal (diameter > 5 μm) and lamellar (eutectic) morphology can be observed. As similar contrast and bimodal size distribution is found for the Ta alloyed materials, but without the lamellar appearance of the smaller particles. With both Mo and W alloyed materials the particles are also of bright contrast, but of much smaller size (diameter < 0.5 μm). In the Mo alloyed samples the particles are partially arranged as lamellae, in the W alloyed materials they appear predominantly on matrix grain boundaries.

Fig. 6 compiles XRD spectra of all Fe–10 B–5 X alloys (in black) together with the fitting results for the given phases (red, green, cyan and pink, respectively) identified within the ferritic Fe matrix (blue; lattice parameter *a* of 0.278 nm determined by the Pawley fit). Pawley analyses of the phases and their lattice parameters obtained besides the matrix phase are listed in Table 2. The XRD investigation identified the particles within Ti, Zr and Hf alloyed samples as TiB_2, ZrB_2 and HfB_2, respectively (all of hexagonal lattice type), in agreement with literature data [9]. Within the V, Nb, Ta and Cr alloyed samples, borides of the tetragonal M_2B structures with similar lattice parameters could be identified. In the V alloyed sample, hexagonal MB_2 phase could identified (most probably VB_2), which likely corresponds to the smaller number of darker particles found in the SEM images (Fig. 5). Ternary NbFeB and TaFeB borides (both hexagonal structure, similar lattice parameters) were identified in the Nb and Ta alloyed materials, respectively. A similar MMB-type phase (FeWB), but with orthorhombic structure, was found in the W alloyed sample, as well as peaks indicating the presence of a tetragonal M_3B phase. The latter type was also found in the Mo alloyed sample, additional to hexagonal MoB_2 and tetragonal Mo_2FeB_2.

5. Discussion

5.1. Microstructure–property relationships of the different Fe–B–X alloys

We successfully screened the stiffness, density, strength and ductility of Fe–10 B–5 X alloys (at.%; X = Ti, Zr, Hf, V, Nb, Ta, Cr, Mo, W) after liquid metallurgy synthesis and thermo-mechanical processing. Our

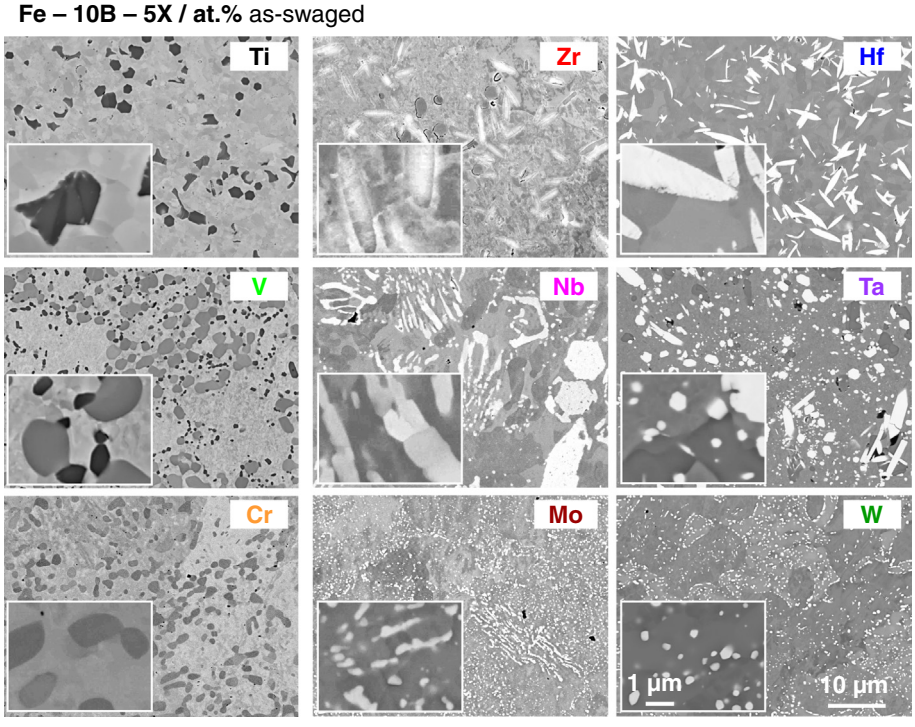

Fig. 5. SEM images (backscatter electron contrast, cross sections) showing the microstructures of the different alloys in as-swaged condition.

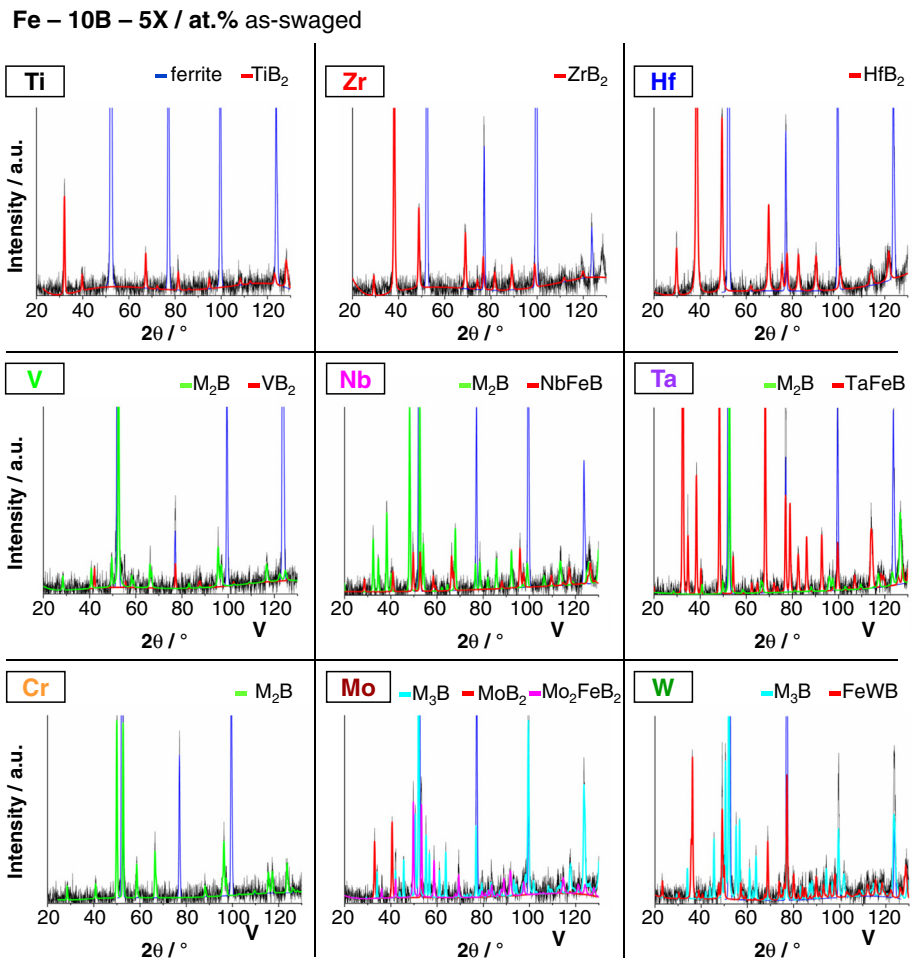

Fig. 6. Measured XRD spectra and fitting results of the different alloys in as-swaged condition.

Table 2
Space groups, lattice parameters (*a*, *b*, *c*) and fitted peak positions (2θ; Pawely fit) of all phases detected in the materials of this study.

Phase	Space group	a (Å)	b (Å)	c (Å)	2θ/°
Ferrite	*Im*-3m	2.866	–	–	52.4; 77.2; 99.7; 123.9
TiB2	*P*6/*mmm*	3.026	–	3.223	32.2; 39.9; 52.2; 67.4; 72.5; 81.3; 81.5; 86.1; 94.9; 108.4; 112.7; 123.2; 128.3; 129.1
ZrB2	*P*6/*mmm*	3.156	–	3.527	29.4; 38.2; 48.9; 61.0; 69.1; 74.3; 76.8; 81.8; 89.2; 99.0; 99.1; 111.8; 120.0
HfB2	*P*6/*mmm*	3.129	–	3.470	29.9; 38.5; 49.5; 62.1; 69.7; 75.5; 77.7; 82.6; 90.3; 100.7; 101.3; 113.8; 114.5; 121.7
VB2	*P*6/*mmm*	2.866	–	3.013	34.5; 42.2; 55.7; 72.9; 77.2; 87.5; 88.0; 92.2; 102.4; 119.0; 125.9
MoB2	*P*6/*mmm*	2.970	–	3.138	33.128; 40.694; 53.441; 69.524; 74.063; 83.567; 83.800; 88.122; 97.456; 112.062; 117.577; 128.128
NbFeB	P-62m	6.000	–	3.199	19.8; 32.5; 34.7; 38.3; 40.3; 48.3; 52.7; 54.2; 62.2; 64.6; 68.0; 71.6; 71.9; 73.2; 76.7; 78.7; 82.1; 82.4; 85.8; 87.0; 92.3; 96.0; 97.2; 99.2; 104.2; 106.4; 109.7; 113.3; 113.6; 114.1; 117.8; 118.8; 125.0; 125.8; 126.9; 129.66; 130.1
TaFeB	P-62m	5.977	–	3.187	19.9; 32.6; 34.8; 38.5; 40.4; 48.5; 52.9; 54.4; 62.5; 64.9; 68.3; 71.9; 72.2; 73.5; 77.1; 79.0; 82.5; 82.8; 86.2; 87.5; 92.8; 96.5; 97.7; 99.7; 104.7; 107.0; 110.3; 114.0; 114.3; 114.7; 118.5; 119.5; 125.9; 126.7; 127.8; 130.6
FeWB	*Pnma*	5.820	3.162	6.807	23.3; 30.5; 35.4; 35.8; 36.4; 39.1; 40.7; 47.7; 49.1; 49.4; 50.1; 51.9; 57.3; 58.1; 59.1; 60.0; 61.2; 63.4; 64.1; 66.4; 67.7; 68.9; 70.1; 73.9; 74.7; 75.0; 75.9; 76.1; 77.2; 77.9; 79.9; 80.2; 82.2; 83.9; 84.0; 84.4; 84.9; 85.2; 87.2; 88.1; 88.7; 89.9; 91.3; 93.0; 93.1; 93.8; 94.1; 95.7; 97.9; 98.1; 101.1; 101.8; 102.3; 102.4; 103.1; 103.9; 104.1; 106.8; 106.9; 108.0; 108.6; 112.1; 112.5; 113.3; 115.5; 115.6; 116.7; 116.8; 117.9; 118.4; 118.6; 119.5; 121.5; 122.3; 123.4; 126.3; 128.2; 128.3; 128.8; 129.0
M2B	*I*4/*mcm*	5.107–5.127	–	4.227–4.255	28.6; 40.8; 49.7; 52.6; 58.3; 59.1 66.2; 67.0; 80.8; 83.1; 87.8; 88.5; 95.5; 95.7; 97.1; 102.6; 109.1; 114.4; 116.7; 122.4; 124.8; 125.6; 125.9; 127.6
M3B	*P*42/*n*	8.626–8.639	–	4.296–4.297	23.9; 26.9; 29.5; 34.1; 34.2; 36.3; 38.3; 42.2; 44.0; 45.7; 49.0; 49.2; 50.7; 50.8; 52.2; 52.4; 55.3; 55.3; 55.4; 56.8; 56.9; 58.2; 61.1; 61.2; 62.6; 63.8; 64.0; 67.9; 68.1; 69.3; 71.8; 72.0; 73.2; 73.3; 74.4; 74.6; 76.9; 77.0; 77.1; 78.6; 79.5; 79.8; 82.0; 82.3; 83.2; 83.4; 83.5; 84.6; 86.9; 87.3; 88.2; 88.3; 88.5; 89.7; 92.0; 93.1; 93.4; 94.3; 94.4; 96.8; 96.9; 97.1; 98.1; 98.2; 98.4; 99.3; 99.6; 101.8; 101.9; 102.1; 103.1; 103.2; 104.3; 108.3; 108.5; 109.5; 109.8; 112.1; 112.8; 113.5; 113.6; 113.8; 114.1; 115.0; 115.5; 117.5; 117.6; 117.7; 117.9; 118.2; 119.0; 119.1; 119.6; 120.8; 123.3; 123.7; 124.0; 125.2; 125.6; 126.3; 126.4; 127.0; 129.4; 129.8; 131.0; 131.2; 131.4
Mo2FeB2	*P*4/*mbm*	5.760	–	3.139	25.4; 33.1; 36.2; 40.6; 42.2; 49.9; 52.1; 53.4; 58.8; 63.1; 68.1; 69.2; 69.4; 75.3; 76.8; 77.8; 79.6; 80.9; 82.4; 83.7; 86.2; 88.0; 89.0; 91.7; 92.0; 97.3; 97.6; 101.9; 104.7; 106.0; 111.6; 113.5; 114.6; 114.9; 117.5; 118.0; 121.2; 122.9; 123.9; 124.1; 127.9; 129.8; 130.9

results allow for the first time to systematically evaluate and compare their microstructures and resultant properties, and thus to gain a first insight into their applicability for the alloy design of novel generations of lightweight structural materials. The reference Ti alloyed material contained about 10 vol.% of TiB_2 in a ferritic Fe matrix (Figs. 5 and 6), which – as the resultant properties (specific modulus ~31 GPa g cm^{-3}; ; YS 420 MPa; UTS 570 MPa; TE 30%; Figs. 2 and 4) – is in excellent agreement with previous findings [28,36]. The other Fe–B–X systems with an identical X/B ratio, synthesis and processing, however, exhibit a wide range of differing particle microstructures (in also ferritic matrices; Figs. 5 and 6), and consequently drastically varying physical and mechanical properties (Figs. 1 and 3).

The Zr alloyed samples showed with 32.5 GPa g^{-1} cm^3 the highest specific modulus of all materials studied here (Fig. 2). It is even exceeding that of the reference material with TiB_2, despite the lower effectiveness of the major particle constituent ZrB_2 (ρ 6.1 g cm^{-3}, *E* 498 to 638 GPa [37]; resulting in a specific modulus of about 82–105 GPa g^{-1} cm^3 compared to 125 GPa g^{-1} cm^3 for TiB_2 [26]). The particles additionally observed in the same microstructure are most likely Fe-rich M_2B borides [8,38] (whose amount was too small to be detected by XRD analysis), which typically exhibit an even lower specific modulus (e.g. Fe_2B: ρ 7.15 g cm^{-3}, *E* 290 GPa [4]), and thus also are most probably not responsible for the increased specific modulus of the Zr alloyed material. However, a pronounced increase in *E* from 233 GPa in the as-cast state to 245 GPa after swaging could be observed (without changes in ρ; Fig. 1). This observation indicates that swaging has promoted alignment of the spiky ZrB_2 particles along the longitudinal axis of the material, resulting in increased stiffness along this direction (anisotropic properties). The associated highly localised stress around the spiky ZrB_2 particulates, however, possibly initiates cracking [27,39], which would explain the observed lower ductility compared to the Ti alloyed samples with its polygonal and round particle morphology (Figs. 3 and 4).

By contrast, the V alloyed samples were stronger but less ductile than the Ti alloyed reference material, which can be attributed to the higher volume fraction of boride particles, which could be identified as VB_2 and M_2B. While the available data for *E* and ρ of VB_2 scatters considerably (ρ ranging from 4.61 to 5.28 g cm^{-3} [37]; experimentally determined *E* 267 GPa [29]; theoretically predicted *E* 562 GPa [40]), they suggest that its specific modulus is most probably smaller than that of TiB_2. As a result, despite the higher fraction of boride particles, the V alloyed materials exhibit a specific modulus on a similar level as the Ti alloyed samples, but at reduced mechanical performance.

The Cr alloyed materials exhibit a similar property profile as the V alloyed samples, yet with slightly better mechanical performance and minimally decreased specific modulus. Here only M_2B type borides were identified in accord with literature data [30,41]. However, the generally beneficial effect of Cr on *E* [42] may have compensated for the absence of typically stiffer MB_2 type borides in this case, i.e. it is likely that Cr_2B (or Cr-rich M_2B) is more effective than Fe_2B, which is to be confirmed by future investigations (for example by targeted nano-indentation experiments as shown in [22]).

Nb alloyed material exhibited with 245 GPa almost as high *E* values as the best performing Zr alloyed samples. Due to the scarcity of information about the intrinsic properties of the detected phases (ρ of hexagonal FeNbB 7.84 g cm^{-3} [41,43]) it remains unclear whether the high specific modulus of the Nb alloyed material is caused by the type or rather the higher volume fraction of the boride phases formed. Their rather detrimental morphology (Fig. 5), however, most probably accounts for the pronounced embrittlement observed for this alloy.

The remaining Mo, Hf, and Ta alloyed materials all exhibited less favourable properties than the above discussed alloy systems. Hf additions resulted in HfB_2 borides of a spiky morphology as for the Zr alloyed material, but nevertheless a much lower specific modulus at similar mechanical performance. Mo and W additions, on the other hand, led to favourable, i.e. very fine and spherical particle morphology of multiple types of phases, but were brittle and, especially for W, extremely ineffective in increasing the specific modulus.

5.2. Consequences for alloy design of HMS

In order to evaluate the different Fe–10 B–5 X alloys with regard to their suitability for alloy design of lightweight structural materials, their respective key properties *E*, ρ, YS and TE are summarised in Fig. 7. Optimum lightweight performance is represented by a simultaneously high specific modulus, YS and TE. Consequently, respective alloy compositions are located in the upper right corner of this modified Ashby map. Four Fe–B–X systems can be readily identified as potential candidates, i.e. those containing Zr, V, Cr, and, as already known, Ti. Within that group, an inverse relationship between mechanical performance and specific modulus applies, just as for strength vs. ductility (Fig. 4) and stiffness vs. density (Fig. 2).

This is related to the respective microstructures with the key parameters phase type (stiffness and density), morphology, size and fraction (assuming strong particle/matrix bonding, which our results showed no adverse indications of). Thus effective yet coarse and spiky particulates of high fraction, for example, are improving the stiffness/density ratio, but at the same time they are deteriorating the plastic mechanical performance. Especially Zr alloyed materials exhibit superior but most probably anisotropic physical properties due to the alignment of the elongated ZrB_2 particles through the thermomechanical processing, but at the price of reduced ductility. However, this phenomenon can also be exploited and rendered beneficial by matching this particle alignment with the loading direction (preferably in the elastic regime) of a specific part as commonly done in fibre reinforced plastics [44]. One pathway to achieve isotropic properties of Fe–B–Zr based HMS could be spheroidisation of ZrB_2 by additional alloying elements, similar in effect to spheroidisation of graphite flakes in grey cast Fe alloys by e.g. by magnesium additions [45]. Alternatively, increased solidification rates during synthesis (for example utilising selective laser deposition as in 3D printing or spray compaction) could be utilised, which has been successfully demonstrated on Fe–Ti–B alloys to result in nano-sized homogeneously distributed particles and superior property combinations [46]. However, as these measures will most likely improve the mechanical performance, the stiffness might be reduced compared to Fe–TiB_2 based HMS due to the lower efficiency of ZrB_2. Our results also reveal Fe–B–Cr alloys as another extremely interesting candidate

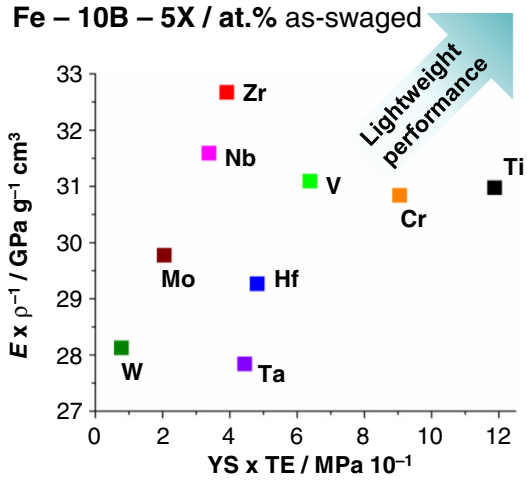

Fig. 7. Modified Ashby map summarising the key material parameters for lightweight performance, i.e. specific modulus (Young's modulus *E* divided by ρ_{bulk} data) as a function of their mechanical performance (Yield strength YS multiplied with tensile elongation TE). Materials with optimum property combinations are located in the upper right corner.

for future HMS design. Their physical and mechanical performance is close to those of Ti-alloyed materials, but with much cheaper alloy composition. Future investigations are aiming at clarifying how higher Cr and B additions and different Cr/B ratios (to match the specific modulus TiB_2 based HMS) affect the microstructure and properties of Fe–B–Cr alloys.

Another promising pathway of balancing physical and mechanical properties is to add more than one boride forming element to Fe–B based alloys. This could be a successful design strategy to circumvent the observed embrittlement by the formation of coarse primary particles [27,28] despite the associated higher particle volume fraction compared to those studied here (about 10 vol.%). For example, an alloy of the composition Fe–20 B–5 Ti–5 Zr (or Cr; all in at.%) might open a thermodynamic state where both pseudo-binary Fe–TiB_2 and Fe–ZrB_2 systems stay below their respective eutectic concentrations (about 12 vol.% of each MB_2 phase). Should the now quaternary composition allow for these phenomena, the resultant fraction of about 10 vol.% each of TiB_2 and of ZrB_2 – both then of small and mechanically compliant eutectic morphology – could thus lead to greatly improved mechanical performance over an alloy containing a similar fraction (20 vol.%) of either only TiB_2 or ZrB_2 with both primary and eutectic boride particles. In a similar manner, rather than combining two boride forming elements, it appears also feasible to replace a given fraction of B for example with C. All these phenomena are the subject of ongoing investigations, as are the influences of additional alloying elements for altering the matrix constitution and microstructure.

6. Summary and conclusions

We systematically screened the mechanical, physical and microstructural properties of nine Fe–10 B–5 X alloy systems (at.%; X = Ti, Zr, Hf, V, Nb, Ta, Cr, Mo, W), all synthesised and processed by standard liquid metallurgical techniques. As precise knowledge about the forming boride phases and their intrinsic properties is rather incomplete, we chose to follow a property driven approach in order to identify the most suitable systems for the alloy design of metal matrix composite steels as next generation lightweight materials. From the obtained stiffness, density and tensile data, as well as their relation to type, size, morphology and dispersion of the formed boride particles, the following conclusions can be drawn:

(1) The Fe–B–Ti alloy, containing ~10 vol.% of TiB_2 in a ferritic Fe matrix, represents with a specific modulus of ~31 GPa g^{-1} cm^3, yield strength of ~420 MPa, ultimate tensile strength of ~570 MPa and ~30% tensile elongation the reference HMS material, in excellent agreement with literature data.

(2) The other Fe–B–X systems exhibited widely differing microstructures of different boride phases and mixes thereof, ranging from spiky MB_2 to spherical M_2B and lamellar borides of more complex morphologies and composition. Both density and stiffness were affected by thermomechanical treatments, up to about 0.2 g cm^{-3} and 10 GPa, respectively, depending on the alloy system.

(3) The property profile of the alloys fall into two groups: Zr, Nb, Cr and V alloyed samples exhibited a specific modulus similar or better than the Ti-alloyed samples but at reduced mechanical performance, or the other way around, respectively. Mo, Hf, Ta and W alloyed systems, on the other hand, neither reached a high stiffness/density ratio, nor high strength and ductility, despite partly favourable boride microstructures and fractions.

(4) Based on these findings Cr and Zr were identified as the most promising boride forming elements for HMS alloy design. Cr, as its high fraction of M_2B borides of spherical morphology allows achieving an almost similar stiffness/density ratio and mechanical performance as Ti alloyed materials, but at greatly reduced alloying costs. Zr alloyed materials on the other hand were softer and less ductile than the reference material, but the alignment of spiky ZrB2 particles during swaging led to a much higher – though most probably anisotropic – specific modulus.

(5) Future investigations are concerned with further iterating the ideal ratio and fraction of Cr and B using bulk metallurgical high throughput techniques. Further interest lies in examining and exploiting the anisotropic properties observed for Zr alloyed materials, and, most importantly, the possibility to combine different boride forming elements for balancing conflicting mechanical and physical properties. This might also be achieved by controlling the solidification kinetics and by utilising additional alloying elements to further improve the property profile of HMS.

Acknowledgements

M. Kulse, B. Breitbach and L. Christiansen are gratefully acknowledged for their support with synthesis, XRD analysis, data evaluation and metallographic preparation.

References

[1] F. Bonnet, V. Daeschler, G. Petitgand, High modulus steels: new requirement of automotive market. How to take up challenge? Can. Metall. Q. 53 (3) (2014) 243–252.
[2] I.A. Ibrahim, F.A. Mohamed, E.J. Lavernia, Particulate reinforced metal matrix composites — a review, J. Mater. Sci. 26 (5) (1991) 1137–1156.
[3] D.J. Lloyd, Particle-reinforced aluminum and magnesium matrix composites, Int. Mater. Rev. 39 (1) (1994) 1–23.
[4] Y. Feng, Strengthening of Steels by Ceramic Phases, Fakultät für Georessourcen und Materialtenik, RWTH Aachen, 2013 169.
[5] A. Evans, C. San Marchi, A. Mortensen, Metal Matrix Composites in Industry - An Introduction and a Survey, Springer US2003.
[6] N. Chawla, K.K. Chawla, Metal Matrix Composites, Springer US2006.
[7] M.F. Ashby, Materials Selection in Mechanical Design, Butterworth-Heinemann, Burlington, MA, 2005.
[8] C. Baron, H. Springer, D. Raabe, Efficient liquid metallurgy synthesis of Fe–TiB2 high modulus steels via in-situ reduction of titanium oxides, Mater. Des. 97 (2016) 357–363.
[9] A.K. Shurin, V.E. Panarin, Phase equilibria and structure of Fe-TiB2, Fe-ZrB2 and Fe-HfB2 alloys, Izvestiya Akademii Nauk SSSR 5 (1974) 235–239.
[10] K. Tanaka, T. Saito, Phase equilibria in TiB2-reinforced high modulus steel, Journal of Phase Equilibria 20 (3) (1999) 207–214.
[11] J.Y. Zhang, Z.Y. Fu, W.M. Wang, H.Y. Wang, X.M. Min, Wettability between TiB2 ceramic and metals, Acta Metall. Sin. 12 (4) (1999) 395–400.
[12] Z. Kulikowski, A. Wisbey, T.M.T. Godfrey, P.S. Goodwin, H.M. Flower, Mechanical properties of high performance lightweight steels, Mater. Sci. Technol. 16 (7–8) (2000) 925–928.
[13] C.C. Degnan, P.H. Shipway, A comparison of the reciprocating sliding wear behaviour of steel based metal matrix composites processed from self-propagating high-temperature synthesised Fe–TiC and Fe–TiB2 masteralloys, Wear 252 (9–10) (2002) 832–841.
[14] C.C. Degnan, P.H. Shipway, The incorporation of self-propagating, high-temperature synthesis-formed Fe-TiB2 into ferrous melts, Metall and Mat Trans A 33 (9) (2002) 2973–2983.
[15] Q.C. Jiang, Y. Wang, H.Y. Wang, B.X. Ma, Z.Q. Zhang, In situ synthesis of TiB2 particulate locally reinforced steel matrix composite by the self-propagating high-temperature synthesis reaction of Al-Fe-Ti-B system during casting, ISIJ Int. 44 (11) (2004) 1847–1851.
[16] A. Anal, T.K. Bandyopadhyay, K. Das, Synthesis and characterization of TiB2-reinforced iron-based composites, J. Mater. Process. Technol. 172 (1) (2006) 70–76.
[17] E. Bayraktar, F. Ayari, D. Katundi, J.P. Chevalier, F. Bonnet, Weldability and Toughness Evaluation of the Ceramic Reinforced Steel Matrix Composites (TIB2-RSMC), 2011 85–92.
[18] L. Cha, S. Lartigue-Korinek, M. Walls, L. Mazerolles, Interface structure and chemistry in a novel steel-based composite Fe–TiB2 obtained by eutectic solidification, Acta Mater. 60 (18) (2012) 6382–6389.
[19] Z. Hadjem-Hamouche, J.P. Chevalier, Y.T. Cui, F. Bonnet, Deformation behavior and damage evaluation in a new titanium diboride (TiB2) steel-based composite, Steel Research International 83 (6) (2012) 538–545.
[20] M. Dammak, I. Ksaeir, O. Brinza, M. Gasperini, Experimental analysis of damage of Fe-TiB2 metal matrix composites under complex loading, 21ème Congrès Français de Mécanique, Bordeaux, 2013.
[21] A. Fedrizzi, M. Pellizzari, M. Zadra, E. Marin, Microstructural study and densification analysis of hot work tool steel matrix composites reinforced with TiB2 particles, Mater. Charact. 86 (2013) 69–79.
[22] R. Fernandez, H. Springer, D. Raabe, In-situ metal matrix composite steels effect of alloying and annealing on morphology, structure and mechanical properties of TiB2 particle containing high modulus steels, Acta Materialia (2015).
[23] S. Lartigue-Korinek, M. Walls, N. Haneche, L. Cha, L. Mazerolles, F. Bonnet, Interfaces and defects in a successfully hot-rolled steel-based composite Fe–TiB2, Acta Mater. 98 (2015) 297–305.

[24] H. Springer, R. Aparicio Fernandez, M.J. Duarte, A. Kostka, D. Raabe, Microstructure refinement for high modulus in-situ metal matrix composite steels via controlled solidification of the system Fe–TiB2, Acta Mater. 96 (2015) 47–56.
[25] Y.Z. Li, Z.C. Luo, H.L. Yi, M.X. Huang, Damage mechanisms of a TiB2-reinforced steel matrix composite for lightweight automotive application, Metallurgical and Materials Transactions E (2016) 1–6.
[26] R.G. Munro, Material properties of titanium diboride, J Res Natl Inst Stan 105 (5) (2000) 709–720.
[27] H. Zhang, H. Springer, R. Aparicio-Fernández, D. Raabe, Improving the mechanical properties of Fe–TiB2 high modulus steels through controlled solidification processes, Acta Mater. 118 (2016) 187–195.
[28] C. Baron, H. Springer, D. Raabe, Effects of Mn additions on microstructure and properties of Fe–TiB2 based high modulus steels, Mater. Des. 111 (2016) 185–191.
[29] G.V. Samsonov, I.M. Vinitskii, Handbook of Refractory Compounds, Springer US1980.
[30] K. Yamada, H. Ohtani, M. Hasebe, Thermodynamic analysis of the Fe-Cr-B ternary system, High Temperature Materials and Processes 27 (4) (2009) 269–284.
[31] H. Springer, D. Raabe, Rapid alloy prototyping: compositional and thermo-mechanical high throughput bulk combinatorial design of structural materials based on the example of 30Mn–1.2C–xAl triplex steels, Acta Materialia 60 (12) (2012) 4950–4959.
[32] P. Eckerlin, H. Kandler, Structure Data of Elements and Intermetallic Phases, Springer, Berlin Heidelberg, 1971.
[33] D. Raabe, H. Springer, I. Gutierrez-Urrutia, F. Roters, M. Bausch, J.B. Seol, M. Koyama, P.P. Choi, K. Tsuzaki, Alloy design, combinatorial synthesis, and microstructure–property relations for low-density Fe-Mn-Al-C austenitic steels, JOM 66 (9) (2014) 1845–1856.
[34] H. Springer, M. Belde, D. Raabe, Bulk combinatorial design of ductile martensitic stainless steels through confined martensite-to-austenite reversion, Mater. Sci. Eng. A 582 (2013) 235–244.
[35] H. Springer, M. Belde, D. Raabe, Combinatorial design of transitory constitution steels: coupling high strength with inherent formability and weldability through sequenced austenite stability, Mater. Des. 90 (2016) 1100–1109.
[36] R. Rana, C. Liu, Effects of ceramic particles and composition on elastic modulus of low density steels for automotive applications, Can. Metall. Q. 53 (3) (2014) 300–316.
[37] P.T.B. Shaffer, Plenum Press Handbooks of High-Temperature Materials - No. 1 Materials Index, Springer US1963.
[38] A. Antoni-Zdziobek, M. Gospodinova, F. Bonnet, F. Hodaj, Solidification paths in the iron-rich part of the Fe–Ti–B ternary system, J. Alloys Compd. 657 (2016) 302–312.
[39] N. Chawla, K.K. Chawla, Microstructure-based modeling of the deformation behavior of particle reinforced metal matrix composites, J. Mater. Sci. 41 (3) (2006) 913–925.
[40] Y.H. Duan, Y. Sun, Z.Z. Guo, M.J. Peng, P.X. Zhu, J.H. He, Elastic constants of AlB2-type compounds from first-principles calculations, Comput. Mater. Sci. 51 (1) (2012) 112–116.
[41] B. Eisenmann, H. Schäfer, Elements, borides, carbides, hydrides · DyB - FeUB, in: K.-H. Hellwege, A.M. Hellwege (Eds.),Elements, Borides, Carbides, Hydrides, Landolt-Börnstein - Group III Condensed Matter 1988, pp. 84–113.
[42] G.R. Speich, A.J. Schwoeble, W.C. Leslie, Elastic constants of binary iron-base alloys, MT 3 (8) (1972) 2031–2037.
[43] T.A. Sviridova, T.R. Chueva, M.V. Gorshenkov, E.V. Shelekhov, N.P. Dyakonova, P.A. Borisova, A new metastable phase in Fe–Nb–B system, J. Alloys Compd. 658 (2016) 525–532.
[44] R.F. Gibson, A review of recent research on mechanics of multifunctional composite materials and structures, Compos. Struct. 92 (12) (2010) 2793–2810.
[45] H. Berns, W. Theisen, Eisenwerkstoffe – Stahl und Gusseisen, Springer, Berlin Heidelberg, 2008.
[46] H. Springer, C. Baron, A. Szczepaniak, V. Uhlenwinkel, D. Raabe, Stiff, light, strong and ductile: nano-structured high modulus steel, Nature materials (2016) under review.